

Second-Generation Phenylthiazole Antibiotics with Enhanced Pharmacokinetic Properties

Mohammed A. Seleem,[†] Ahmed M. Disouky,[†] Haroon Mohammad,[‡] Tamer M. Abdelghany,[§] Ahmed S. Mancy,^{||} Sammar A. Bayoumi,[⊥] Ahmed Elshafeey,^{#,∇} Ahmed El-Morsy,[†] Mohamed N. Seleem,^{‡,⊗} and Abdelrahman S. Mayhoub^{*,†}

[†]Department of Pharmaceutical Organic Chemistry, College of Pharmacy, Al-Azhar University, Cairo 11884, Egypt

[‡]Department of Comparative Pathobiology, Purdue University, College of Veterinary Medicine, West Lafayette, Indiana 47907, United States

[§]Department of Pharmacology, College of Pharmacy, Al-Azhar University, Cairo 11884, Egypt

^{||}Department of Clinical Pharmacy, College of Pharmacy, Heliopolis University, Cairo 11777, Egypt

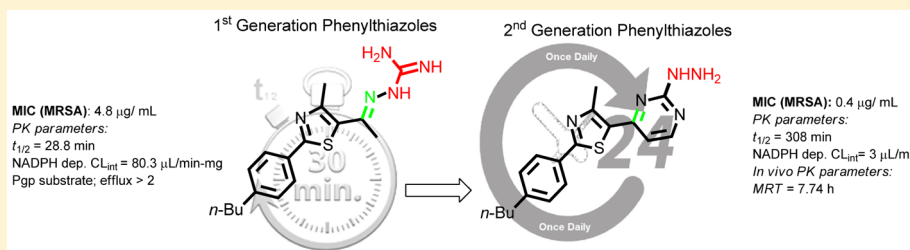
[⊥]Department of Pharmaceutics, College of Pharmacy, Heliopolis University, Cairo 11777, Egypt

[#]Bioequivalence Section, Genuine Research Center, Heliopolis, Cairo 11757, Egypt

[∇]Department of Pharmaceutics & Industrial Pharmacy, Faculty of Pharmacy, Cairo University, Kasr El-Ainy, Cairo 11562, Egypt

[⊗]Purdue Institute for Inflammation, Immunology, and Infectious Diseases, Purdue University, West Lafayette, Indiana 47907, United States

S Supporting Information



ABSTRACT: A series of second-generation analogues for 2-(1-(2-(4-butylphenyl)-4-methylthiazol-5-yl)ethylidene)amino-guanidine (**1**) have been synthesized and tested against methicillin-resistant *Staphylococcus aureus* (MRSA). The compounds were designed with the objective of improving pharmacokinetic properties. This main aim has been accomplished by replacing the rapidly hydrolyzable Schiff-base moiety of first-generation members with a cyclic, unhydrolyzable pyrimidine ring. The hydrazide-containing analogue **17** was identified as the most potent analogue constructed thus far. The corresponding amine **8** was 8 times less active. Finally, incorporating the nitrogenous side chain within an aromatic system completely abolished the antibacterial character. Replacement of the *n*-butyl group with cyclic bioisosteres revealed cyclohexenyl analogue **29**, which showed significant improvement in *in vitro* anti-MRSA potency. Increasing or decreasing the ring size deteriorated the antibacterial activity. Compound **17** demonstrated a superior *in vitro* and *in vivo* pharmacokinetic profile, providing compelling evidence that this particular analogue is a good drug candidate worthy of further analysis.

INTRODUCTION

Infections caused by multidrug-resistant bacteria have become a global public health crisis. In particular, infections due to multidrug-resistant staphylococci have been increasing at an alarming rate. Clinically, *Staphylococcus aureus* was once susceptible to most antibiotics. However, the emergence of antibiotic resistance in *S. aureus* has occurred as a series of waves. Starting in the mid-1940s,^{1–3} isolates of *S. aureus* were discovered that produced a plasmid-encoded penicillinase capable of hydrolyzing the β -lactam ring of penicillin, thus rendering the antibiotic ineffective. Penicillin-resistant strains shortly began to cause community infections, and by the early 1950s they had become pandemic.⁴ The first reports of a

methicillin-resistant *S. aureus* strain—known as MRSA—were published in 1961.^{3,5} Outbreaks of infections caused by different MRSA strains were reported in hospitals in the United States in the late 1970s; by the 1980s these strains were endemic,^{6,7} leading to the worldwide pandemic of MRSA in hospitals that continues today. Although global in its distribution and impact, MRSA was still confined mostly to healthcare facilities. In 2013, the Centers for Disease Control and Prevention (CDC) reported that more than 11 000 people died from MRSA-related infections in the United States alone.⁸

Received: February 15, 2016

Egypt is among several Mediterranean countries that are experiencing a surge in MRSA infections.⁹ The prevalence of MRSA in both Egyptian community and hospital-acquired pyogenic skin and soft tissue infections is currently alarming.¹⁰

Over the past 40 years, the ever-increasing burden of MRSA infections led to the increased use of vancomycin, an agent of last resort for treatment of recalcitrant MRSA infections. This intensive, selective pressure resulted in the emergence of vancomycin-intermediate *S. aureus* (VISA)¹¹ and vancomycin-resistant *S. aureus* (VRSA) isolates.¹² Compounding the problem further, the effectiveness of vancomycin is limited by prolonged, persistent, or recurrent bacteraemia during therapy,^{13,14} high rates of microbiological and clinical failures,¹⁵ nephrotoxicity,¹⁶ and the increasing prevalence of non-susceptible strains.^{14–17}

In addition to exhibiting resistance to vancomycin, MRSA isolates resistant to a wide variety of antibacterial classes, including the β -lactam antibiotics,¹⁸ macrolides,¹⁹ and fluoroquinolones,^{19–22} have been found. Collectively this points to the pressing need to develop novel antimicrobial agents. These new agents must have enhanced pharmacokinetic (PK) properties in order to be useful for clinical applications.

In the search for novel antimicrobials, phenylthiazoles carrying a nitrogenous moiety at one end and a lipophilic part at the opposite side (Figure 1) were previously reported as

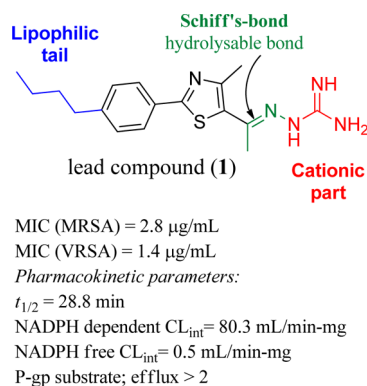


Figure 1. MIC values and pharmacokinetic profile of lead structure 1. Two important structural features are colored: red indicates the nitrogenous part, and blue indicates the lipophilic tail.

new antimicrobial scaffolds with potent activity against multidrug-resistant strains of *S. aureus*, including MRSA and VRSA.²³ These phenylthiazole antibacterials possess a selective advantage over vancomycin in their ability to rapidly eradicate a high inoculum of MRSA.²³ This is clinically significant for the treatment of diseases caused by staphylococci, as it will impact the size and timing of doses administered to MRSA-infected patients.^{24,25} The highly promising *in vivo* antimicrobial activity of the discovered phenylthiazole class of antibacterials, either as a single agent or in combination with other therapeutic agents,^{26,27} has thus far been hampered by their poor PK profile. For instance, the lead compound 2-(1-(2-(4-butylphenyl)-4-methylthiazol-5-yl)ethylidene)aminoguanidine (1, Figure 1) is rapidly cleared by human liver microsomes, resulting in a relatively short half-life (<30 min).^{23,26} Designing compounds with a longer duration is important to ensure the active compound stays in circulation long enough to reach the target site of infection and exert its antibacterial effect.

In this article, a strategy is proposed to overcome the metabolic instability of the aminoguanidine moiety utilizing ligand-based drug design approaches, given that the exact molecular target of these phenylthiazoles has not been identified yet. To date, all first-generation phenylthiazoles carry a hydrolyzable C=N linkage (Figure 2), which

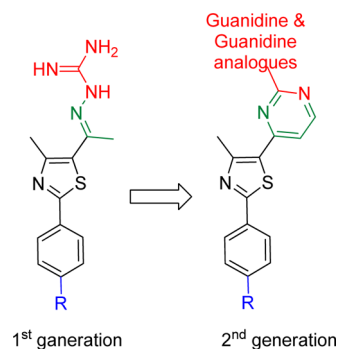


Figure 2. New design.

contributes to their metabolic instability and short $t_{1/2}$. All attempts to replace the hydrolyzable C=N with more metabolically stable C-N or amide bonds resulted in less active compounds.²⁸ These results, collectively, pointed to the importance of “linker conformational restriction”. Therefore, in this study, we propose that incorporating the hydrolyzable Schiff's base moiety within an aromatic ring system will enhance the overall metabolic stability of the phenylthiazoles while keeping the required conformational restriction. Thus, several phenylthiazoles bearing, at thiazole position-5, a pyrimidine ring connected with guanidine, or a guanidine-like moiety, have been proposed (Figure 2).

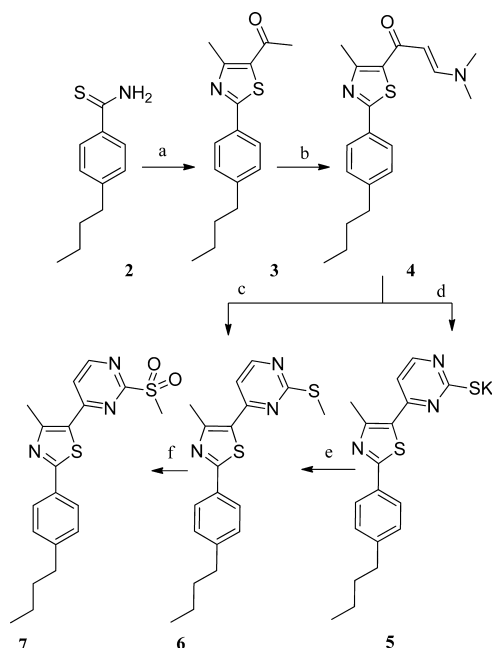
RESULTS AND DISCUSSION

Chemistry. Thioamide 2 was treated with α -chloroacetylacetone to yield phenylthiazole derivative 3 (Scheme 1). The latter compound was allowed to react with dimethylformamide–dimethylacetal (DMF-DMA) to give the first key intermediate, 4. Finally, the methylsulfonyl derivative 7 was easily obtained by allowing enaminone 4 to react with thiourea, followed by methylation and oxidation of the free thiol group as detailed in Scheme 1.

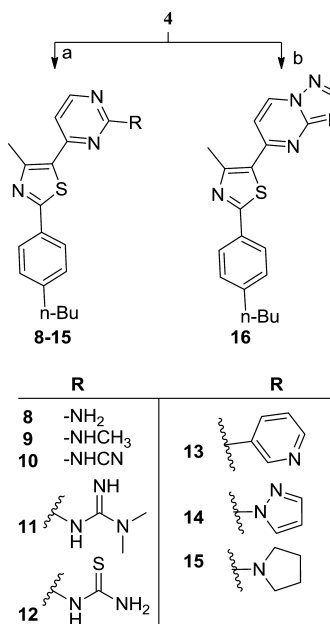
The enaminone moiety of compound 4 revealed two distinct doublet signals in the ^1H NMR spectrum at δ 7.69 and 5.44, each of one proton, with coupling constant of 12 Hz, characteristic of the *E*-configuration. Upon cyclization of compound 5, the chemical shifts of those two signals were shifted to a higher field, and their *J* value decreased to around 5 Hz. The inserted *S*-methyl group of compound 6 was represented in the ^1H NMR spectrum by one extra singlet signal in the aliphatic region at δ 2.55. This signal was shifted downfield to δ 2.93 upon oxidation of the *S*-mercaptyl group into the methylsulfonyl analogue 7.

With enaminone key intermediate 4 in hand, nine 5-pyrimidinylphenylthiazoles were obtained via reaction with different nucleophiles (Scheme 2).

Finally, methylsulfonyl intermediate 7 was utilized to complete this series of optimized phenylthiazoles at position-5. Hence, the methylsulfonyl moiety was replaced by three nucleophiles, namely, hydrazine hydrate, guanidine hydro-

Scheme 1. Synthesis of Key Intermediates 4 and 7^a

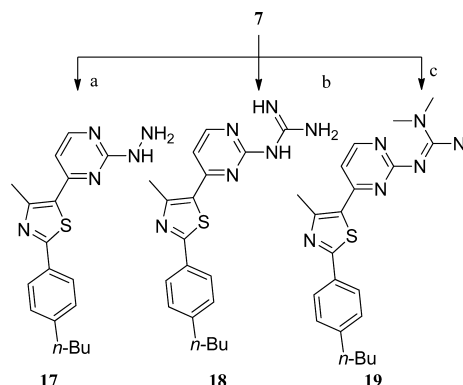
^aReagents and conditions: (a) absolute EtOH, 3-chloropentane-2,4-dione, heat to reflux, 12 h; (b) DMF-DMA, heat at 80 °C, 8 h; (c) *S*-methylisothiurea hemisulfate, K₂CO₃, EtOH, heat to reflux, 6 h; (d) thiourea, KOH, EtOH, heat to reflux, 8 h; (e) dimethyl sulfate, KOH, H₂O, stirring at 23 °C, 12 h; (f) MCPBA, dry DCM, stirring at 23 °C, 16 h.

Scheme 2. Synthesis of Compounds 8–16^a

^aReagents and conditions: (a) appropriate guanidine, K₂CO₃, absolute EtOH, heat to reflux, 8 h; (b) 4*H*-1,2,4-triazol-3-amine, absolute EtOH, heat to reflux for 5 h.

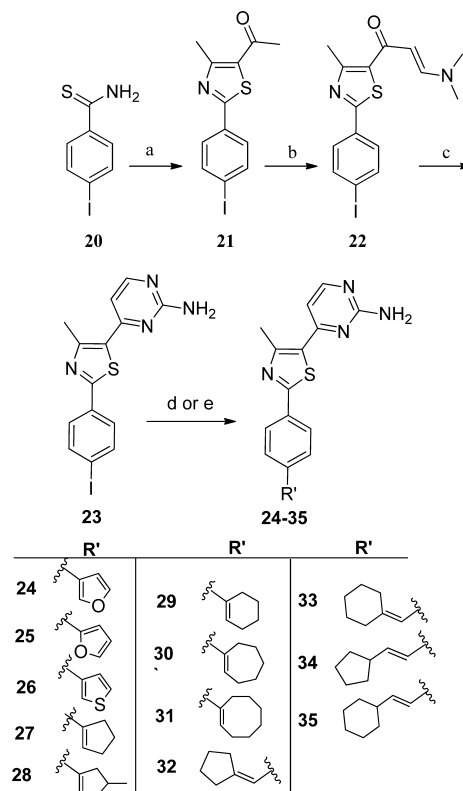
chloride, and tetramethylguanidine, to afford the final products 17–19, respectively (Scheme 3).

The *para*-iodo intermediates 21 and 22 necessary for the subsequent chemical transformations (compounds 23–35)

Scheme 3. Synthesis of Compounds 17–19^a

^aReagents and conditions: (a) NH₂NH₂·H₂O, DMF, heat at 80 °C for 0.5 h; (b) guanidine hydrochloride, DMF, heat at 80 °C for 2 h; (c) tetramethylguanidine, DMF, heat at 80 °C for 2 h.

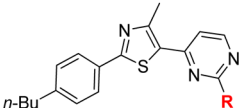
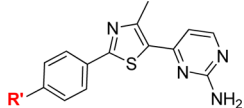
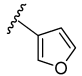
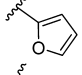
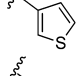
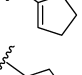
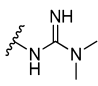
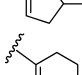
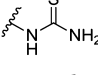
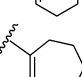
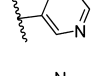
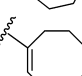
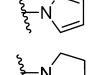
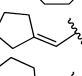
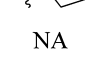
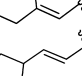
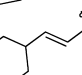

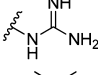

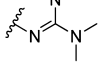
have been synthesized in a similar manner as the corresponding *n*-butyl analogues 4 and 7, as detailed in Scheme 4.

Scheme 4. Synthesis of Compounds 24–35^a

^aReagents and conditions: (a) absolute EtOH, 3-chloropentane-2,4-dione, heat to reflux, 12 h; (b) DMF-DMA, 100 °C, 8 h; (c) guanidine hydrochloride, K₂CO₃, EtOH, heat to reflux, 12 h; (d) boronic acid derivative, Xphos Pd G2, dry DMF, K₂CO₃, 85 °C, MW, 1 h; (e) proper alkene, dry DMF, Pd(OAc)₂, Et₃N, 80 °C, 2 h.

So far, three aromatic analogues to the *n*-butyl moiety have been obtained via Suzuki cross-coupling using the second-generation pre-made Xphos Pd catalyst (Scheme 4). The ¹H NMR spectra of compounds 24–26 showed three extra signals each, in the aromatic region, corresponding to the furyl and/or thienyl moieties (see Experimental Section).

Table 1. Antimicrobial Activity ($\mu\text{g/mL}$) of Second-Generation Phenylthiazoles vs MRSA (2658 RCMB)^a

							
Entry	R	Cpd	MIC \pm SD ($\mu\text{g/mL}$)	Entry	R'	Cpd	MIC \pm SD ($\mu\text{g/mL}$)
1	NA	1	4.8 ± 0.0	16	I	23	> 25
2	NA	4	> 25	17		24	7.8 ± 0.5
3	-NH ₂	8	3.12 ± 0.10	18		25	8.7 ± 0.3
4	-NHCH ₃	9	> 25	19		26	6.25 ± 0.0
5	-NHCN	10	18.7 ± 2.3	20		27	3.12 ± 0.00
6		11	0.78 ± 0.00	21		28	3.8 ± 0.4
7		12	> 25	22		29	0.78 ± 0.00
8		13	17.2 ± 0.4	23		30	3.12 ± 0.00
9		14	> 25	24		31	5.60 ± 0.10
10		15	> 25	25		32	1.17 ± 0.19
11	NA	16	> 25	26		33	1.56 ± 0.00
12	-NH-NH ₂	17	0.40 ± 0.0	27		34	3.12 ± 0.00
13		18	1.56 ± 0.10	28		35	3.12 ± 0.00
14		19	> 25	29	Van.	Van.	1.56 ± 0.00

^aVan. = vancomycin.

On the other hand, a series of cycloalkenes have been tethered to the phenyl group's *para*-position via Heck cross-coupling using a standard protocol, i.e., palladium acetate and triethylamine in a dry DMF (Scheme 4). Similarly, four terminal alkenes have been allowed to react with the 4-iodophenylthiazole **23** using the same protocol (Scheme 4).

Biological Results. A. Anti-MRSA Activity. At the outset of our study, the hypothesis of replacing the hydrolyzable Schiff's moiety with a pyrimidine ring was first tested by synthesizing the simplest second-generation derivative with an aminopyrimidine group at the thiazole position-5. So far, the aminopyrimidine derivative **8** inhibited MRSA at a value ($3.12 \pm 0.10 \mu\text{g/mL}$) slightly better than that of the first-generation lead compound **1**, which had a minimum inhibitory concentration (MIC) value of $4.8 \mu\text{g/mL}$ against the same MRSA strain (Table 1). Fortunately, the intrinsic $t_{1/2}$ of the first derivative in the second generation was 7 times (195 min, Table 2) higher than that of the lead compound **1** (28.8 min, Table 2).

Table 2. Evaluation of Metabolic Stability of Tested Compounds, Verapamil, and Warfarin in Human Liver Microsomes^a

tested compd	NADPH-dependent		NADPH-free	
	CL _{int} ($\mu\text{L}/\text{min}\cdot\text{mg}$)	$t_{1/2}$ (min)	CL _{int} ($\mu\text{L}/\text{min}\cdot\text{mg}$)	$t_{1/2}$ (min)
1 ²³	80.3	28.8	0.5	>60
8	3.3	195	0.5	>60
11	7.5	243	0.5	>60
17	3	308	0.5	>60
verapamil	201	11	1	>60
warfarin	0.3	>60	0.0	>60

^aCL_{int} = microsomal intrinsic clearance; $t_{1/2}$ = half-life.

With this solid evidence in hand, we replaced the free amino group with different nitrogenous moieties in order to address the structure–activity relationships (SARs) around what was identified previously as “the cationic part”. Adding a methyl

group to the terminal nitrogen (compound **9**) or nitrile group (compound **10**) dramatically decreased the antibacterial activity, mostly due to the poor solubility issues under the testing conditions.

Next, the guanidine-like moiety of **8** was replaced with a true guanidinyll group, and compound **18** was prepared. The antibacterial activity of **18** was on par with that of vancomycin, the drug of choice for treatment of systemic MRSA infections; both compounds possessed a MIC value of 1.56 $\mu\text{g/mL}$ (Table 1). This value is 3 times better than that of lead compound **1** and 2-fold better than that of the first lead in the second generation (compound **8**). Altering the lipophilic properties of compound **18** by replacing the NH with a sulfur atom (compound **12**) led to complete abolishment of the anti-MRSA activity (Table 1). On the other hand, decreasing the polarity of the guanidinyll moiety by adding two methyl groups (compound **11**) ameliorated the antibacterial activity and provided the first derivative in this series with a MIC value below 1 $\mu\text{g/mL}$. This observation sheds light on a possible favorable lipophilic region around the terminal nitrogen. This hypothesis was explored with the simplest derivative in this set of compounds (compound **8**) by incorporating the free amine within a pyrrolidine ring (compound **15**). Unfortunately, the pyrrolidinyll derivative **15** lacks any antibacterial activity. This second observation provided insight into the importance of having a “hydrogen-bond donor” (HBD) within the cationic part. Moving back to the 2-guanidinyllpyrimidine scaffold, the tetramethylguanidine derivative **19** was synthesized to test the latter hypothesis. Unlike the guanidine derivative **18**, the corresponding tetramethyl analogue **19** revealed no antibacterial efficacy (Table 1). This observation confirms our second hypothesis of the importance of having a HBD within the nitrogenous side chain is necessary for anti-MRSA activity.

Inspired by the previous results, a second HBD was added to the amino group of compound **8** and the hydrazoneyl analogue **17** was prepared, which inhibited the growth of MRSA at 0.4 $\mu\text{g/mL}$ (Table 1). The hydrazoneyl derivative **17** demonstrated a 12-fold improvement in its MIC value when compared with the lead compound **1** and was 8 times more active than the first derivative in the second-generation phenylthiazole antibiotics (compound **8**). The antibacterial activity of **17** was further evaluated against a panel of MSSA, MRSA, and VRSA clinical isolates (Table 3), and it was highly comparable with that of vancomycin and linezolid. In addition, compound **17** showed drastic superiority with vancomycin-resistant strains (VRSA10

Table 3. Minimum Inhibitory Concentration (MIC, $\mu\text{g/mL}$) and Minimum Bactericidal Concentration (MBC, $\mu\text{g/mL}$) of Compound 17, Vancomycin, and Linezolid Screened against a Panel of *S. aureus* and Vancomycin-Resistant *Enterococcus faecium* (VRE) Clinical Isolate Strains

	17		vancomycin		linezolid	
	MIC	MBC	MIC	MBC	MIC	MBC
NRS72 (MSSA)	2	8	2	2	1	2
NRS119 (MRSA)	2	2	1	1	32	>64
NRS123 (MRSA USA400)	2	2	1	1	1	16
NRS382 (MRSA USA100)	2	4	1	1	1	8
NRS383 (MRSA USA200)	2	2	1	1	1	32
NRS384 (MRSA USA300)	2	2	1	1	1	4
VRSA10	1	2	>64	>64	1	2
VRE ATCC 700221	2	8	>64	>64	1	32

and VRE ATCC 700221). Subsequent aromatization of the hydrazoneyl moiety provided pyrazolylpyrimidine analogue **14** or its pyridinylpyrimidine derivative **13** that exhibited no antibacterial activity. This observation further confirms our previous assumption that the “nitrogenous side chain has to include, at least, one HBD”.

The main drawback of several commercial antimicrobials used to treat MRSA infections is that they are bacteriostatic (such as linezolid); i.e., they have the ability of inhibiting bacterial growth but do not kill the bacteria, or they exhibit a very slow bactericidal mode of action (such as vancomycin), resulting in difficulty in clearing an infection.^{29,30} An antibacterial agent that demonstrates the ability to rapidly eradicate MRSA would reduce the likelihood of rapid bacterial resistance emerging to this agent. To examine the antibacterial activity of the most promising analogues constructed thus far, a time–kill assay was performed using the most active compound **17** tested against MRSA USA300 strain. This strain is responsible for most cases of community-acquired MRSA (CA-MRSA) infections, MRSA skin and soft tissue infections (SSTIs) in the United States³¹ and other countries around the world,³² and pneumonia as well.³³ Figure 3 represents the elimination rate of

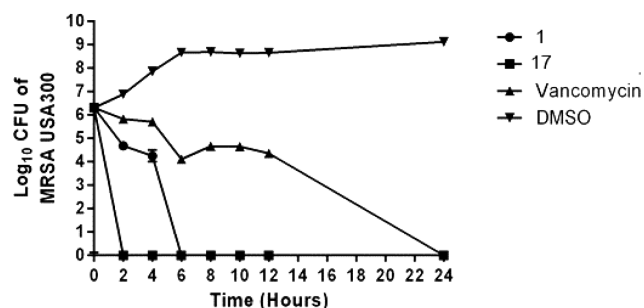


Figure 3. Time–kill analysis of lead compound **1**, compound **17**, and vancomycin at $3.0 \times \text{MIC}$ against methicillin-resistant *Staphylococcus aureus* (MRSA) strain USA300 over a 12 h incubation period at 37 °C. DMSO served as the control. Values were obtained from triplicate samples used for each compound studied.

compound **17** in comparison with vancomycin and lead compound **1**. The lead compound **1** required 6 h to logarithmically reduce the MRSA inoculum to zero colony forming units (CFU), while vancomycin required 24 h to achieve the same effect. Interestingly, the second-generation phenylthiazole derivative **17** rapidly eliminated the bacterial cells within a 2 h window. These data confirm that the second-generation phenylthiazoles maintained the selective advantage observed with the first-generation compounds over vancomycin and linezolid in terms of rate of elimination of MRSA cells.

After tuning the proper cationic part, we next directed our attention toward the lipophilic tail at the phenyl ring’s *para*-position, since this part has been previously established to have a profound impact on the antibacterial activity of the phenylthiazole compounds.^{23,28} Thus far, the SAR at phenyl position-4 has been studied, and the *n*-butyl moiety of the second-generation lead compound **8** has been replaced with different conformationally restricted bioisosteres in order to rigorously explore the SAR at this position.

As a prologue to this new set of structure optimizations, the intermediate **23**, carrying an iodine atom in place of the *n*-butyl moiety, was found to lack antibacterial activity (Table 1). This preliminary observation further highlights the importance of the

lipophilic tail. Next, three aromatic bioisosters, **24–26**, each with four carbon units, were prepared and revealed less anti-MRSA activity. In addition to their reduced potency, the aromatic derivatives **24–26** also possessed poor aqueous solubility (Table 4). These results encouraged us to move to

Table 4. Evaluation of Solubility of Tested Compounds, Reserpine, Tamoxifen, and Verapamil in Phosphate-Buffered Saline

compd tested	solubility limit (μM) ^a
lead compound 1	62.5
8	42
11	53
17	55
24	13
25	14
26	8.5
27	35
29	37
reserpine	31.3
tamoxifen	15.6
verapamil	>500

^aSolubility limit corresponds to the highest concentration of test compound where no precipitate was detected (OD540).

examine the alicyclic analogues. Therefore, a series of cycloalkenyl-containing derivatives, **27–31**, were prepared, and their MICs against MRSA (Table 1) were also evaluated using the broth microdilution method, in accordance with the recommendations contained in the CLSI guidelines.³⁴

To date, the optimal number of carbon units has been found to be six. Hence, compound **29**, with a cyclohexenyl side chain, was able to inhibit MRSA growth at a concentration of 0.78 $\mu\text{g}/\text{mL}$ (1-fold less than the reference drug vancomycin and 4 times better than the second-generation lead compound **8**). Shrinking the substituent's ring size at the phenyl group's *para*-position led to the cyclopentenyl derivative **27** that was on par with the corresponding *n*-butyl lead structure **8** in terms of MIC value (Table 1). Furthermore, adding one extra methyl group, to structurally resemble the cyclohexenyl moiety (compound **28**), further impacted the antibacterial potency in a negative manner (Table 1). The same trend of increasing MIC values was observed by expanding the ring size from six to seven carbon units, and the cycloheptenyl derivative **30** was 4 times less active than the corresponding cyclohexenyl analogue, **29**. Further expanding the ring size generated a less active derivative: the octenyl **31** had a MIC value of 5.6 $\mu\text{g}/\text{mL}$ (Table 1).

We then examined the optimal distance between the cyclic moiety at the phenyl 4-position and phenylthiazole scaffold. At this stage of structural optimization, both cycloheptenyl and cyclooctenyl derivatizations were excluded on the basis of their previously limited antimicrobial potency. Thus, only derivatives with a smaller ring size (cyclohexenyl and cyclopentenyl) were considered. Four derivatives were synthesized, two with one carbon linker (compounds **32** and **33**) and two with a two-carbon units linker (compounds **34** and **35**). The two cycloalkylenemethyl derivatives **32** and **33** were generally more active than the corresponding cycloalkylvinyl analogues **34** and **35** (Table 1). However, the compounds **32** and **33** were as active as vancomycin against MRSA cells; they both were less

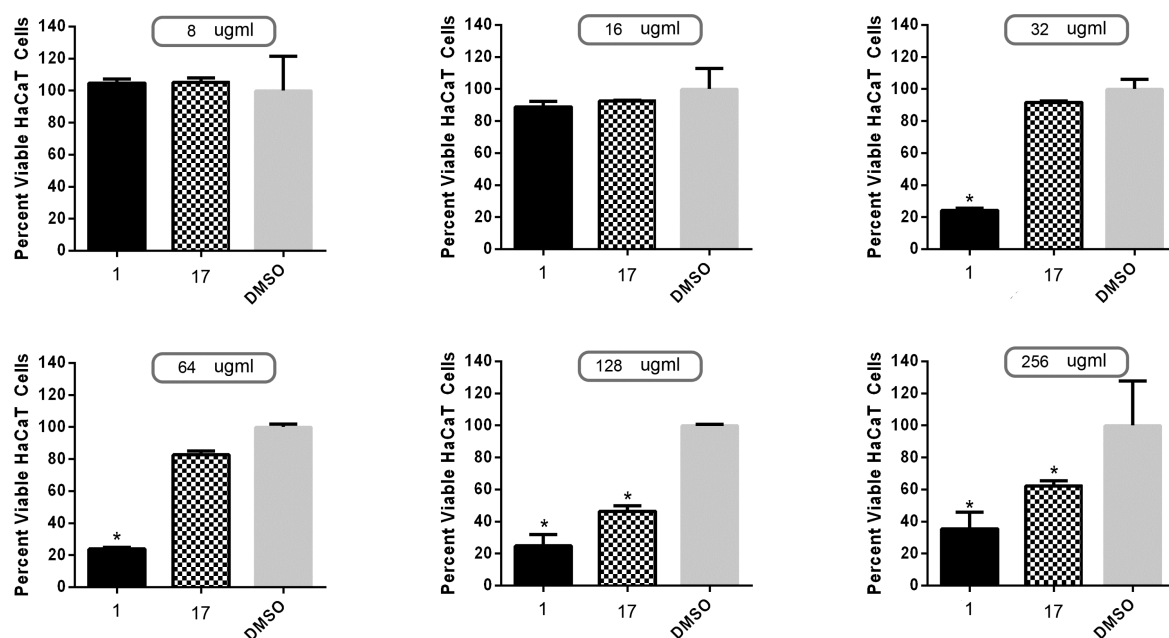


Figure 4. Toxicity analysis of lead compound and second-generation phenylthiazole derivative **17** against human keratinocytes (HaCaT). Percent viable mammalian cells (measured as average absorbance ratio (test agent relative to DMSO)) for cytotoxicity analysis of thiazole compounds **1** and **17** (tested in triplicate) at 8, 16, 32, 64, 128, and 256 $\mu\text{g}/\text{mL}$ against HaCaT cells using the MTS [3-(4,5-dimethylthiazol-2-yl)-5-(3-carboxymethoxyphenyl)-2-(4-sulfophenyl)-2H-tetrazolium] assay. Dimethyl sulfoxide (DMSO) was used as a negative control to determine a baseline measurement for the cytotoxic impact of each compound. The absorbance values represent an average of a minimum of three samples analyzed for each compound. Error bars represent standard deviation values for the absorbance values. A two-way ANOVA, with post hoc Dunnett's multiple comparisons test, determined statistical difference between the values obtained for each compound and DMSO (denoted by the asterisk, $P < 0.05$).

potent than the cyclohexyl analogue **29**, which revealed the best activity in this series (Table 1).

B. Cytotoxicity. The cytotoxicity impact of the second-generation compounds, represented by the most potent derivative **17**, was analyzed against human keratinocytes (HaCaT) and compared with the first-generation compounds, represented by the lead compound **1**. The results are summarized in Figure 4. Compound **1** was nontoxic up to a concentration of 16 $\mu\text{g/mL}$. The toxicity profile of the second-generation derivative **17** showed significant improvement, as it was not toxic up to a concentration of 64 $\mu\text{g/mL}$, which is 160 times more than the MIC value found against MRSA (Figure 4).

C. Physicochemical Properties and Pharmacokinetic Profiling. Thus far, the newly developed second-generation derivatives displayed improved antibacterial activity and an enhanced safety profile in relation to the first-generation compounds. We next moved to examine the “drug-like” properties of the most promising candidate to determine its suitability for further investigation. Drug discovery is a complex process that includes multiple lines of investigation, often with conflicting goals, that necessitates data integration in order to achieve a balanced clinical candidate. Those candidates must possess good PK profiles and physicochemical properties. In this regard, the solubility and apparent permeability of some selected members of the second-generation series of compounds were examined in comparison with those of the lead compound **1** and reference drug molecules. Table 4 demonstrates that tethering the cationic part of the phenylthiazole moiety via a pyrimidine ring resulted in a considerable decrease in aqueous solubility. The aminopyrimidine derivative **8** was found to be 32% less soluble than the lead compound **1** (Table 4). Expanding the polar surface area of the cationic part via replacement of the free amino group of **8** with a hydrazide or guanidine moiety had a positive impact, improving the compound's aqueous solubility as measured by the turbidometric solubility assay. Hence, the aqueous solubility increased from 42 μM in the case of compound **8** to 53 and 55 μM in the case of compounds **11** and **17**, respectively (Table 4); both values are still below that of lead compound **1** but better than those of the two tested FDA-approved drugs, tamoxifen and reserpine (Table 4).

Aqueous solubility is not the only factor that determines oral bioavailability; permeability has also a great impact. In the present work, the Caco-2 bidirectional permeability assay was used to examine the permeability profile of the lead compound in this series, compound **8**, relative to that of the first-generation lead structure, **1**. The values obtained were compared with those from two control drugs, one with limited permeability properties (ranitidine) and one with a strong permeability profile (warfarin). Although compound **8** did possess as strong a permeability profile as warfarin, it exhibited a notable improvement relative to the previously reported poor permeability properties of the lead compound **1** (Table 5). The Caco-2 apparent permeability, $P_{\text{app}}(\text{A} \rightarrow \text{B})$, was significantly improved from 0.0 in the case of **1** to $14.9 \times 10^{-6} \text{ cm/s}$ with compound **8**. In the same vein, the $P_{\text{app}}(\text{B} \rightarrow \text{A})$ value also improved by a factor of 14. These results collectively point out the superiority of the second-generation phenylthiazoles over the older first-generation analogues.

It has already been reported that the lead compound **1** was cleared by liver microsomes at a rate of 80.3 $\mu\text{L/min-mg}$ and had a half-life just below 0.5 h.²³ In this study, the three tested

Table 5. Evaluation of Apparent Permeability of Tested Compounds, Ranitidine, and Warfarin via the Caco-2 Permeability Assay

compd tested	mean P_{app} ($\times 10^{-6} \text{ cm/s}$)		efflux ratio ^c
	A \rightarrow B ^a	B \rightarrow A ^b	
lead compound 1 ²³	0.0 ^d	1.2	>2
8	14.9	17.0	1.1
17	1.6	2.8	1.8
ranitidine	0.2	1.7	8.5
warfarin	27.6	11.1	0.4

^aMean apparent permeability of test compound from apical to basolateral surface. ^bMean apparent permeability of test compound from basolateral to apical surface. ^c $P_{\text{app}}(\text{B} \rightarrow \text{A})/P_{\text{app}}(\text{A} \rightarrow \text{B})$. ^dCompound not detected in receiver compartment (peak below limit of detection); permeability may be underestimated.

compounds, **8**, **11**, and **17**, one from each subclass, were found to possess metabolic clearance rates ranging between 3 and 7.5 $\mu\text{L/min-mg}$ (Table 2). These values denote that second-generation phenylthiazoles exhibit 10- to 27-fold improvements in how rapidly they are metabolized and cleared from liver cells compared to the first-generation compounds.

Encouraged by the promising *in vitro* results, we determined the PK parameters of the most promising candidate thus far, compound **17**, using Sprague–Dawley (SD) rats. Three animals were dosed with compound **17** (50 mg/kg) orally, and plasma samples were collected over a 24 h period. The preliminary PK curve (Figure 5) suggests a once daily dose.

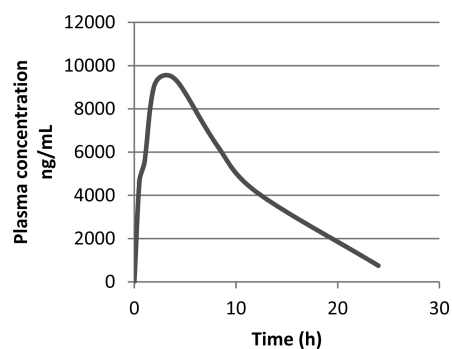


Figure 5. Oral pharmacokinetic curve in rat after 50 mg/kg oral dose of compound **17**.

Interestingly, compound **17** was detected in plasma in a microgram range ($C_{\text{max}} = 9.3 \mu\text{g/mL}$), well above the MIC value, which reflects the good permeability and absorption properties determined from the Caco-2 permeability and turbidometric solubility analysis described above. The *in vivo* mean residence time (MRT) for **17** was approximately 8 h (Table 6). Finally, these data collectively provide solid evidence that this new generation of phenylthiazoles, unlike previously

Table 6. Compound 17 Plasma Pharmacokinetic Parameters Following Single Oral Dose (50 mg/kg) to Rats

C_{max} (ng/mL)	9326.32	AUC_{tot} (h·(ng/mL))	100010.96
t_{max} (h)	4.67	t_{half} (h)	8.24
AUC_{last} (h·(ng/mL))	83173.60	MRT (h) ^a	7.74
λ_z (1/h)	0.19		

^aMean residence time.

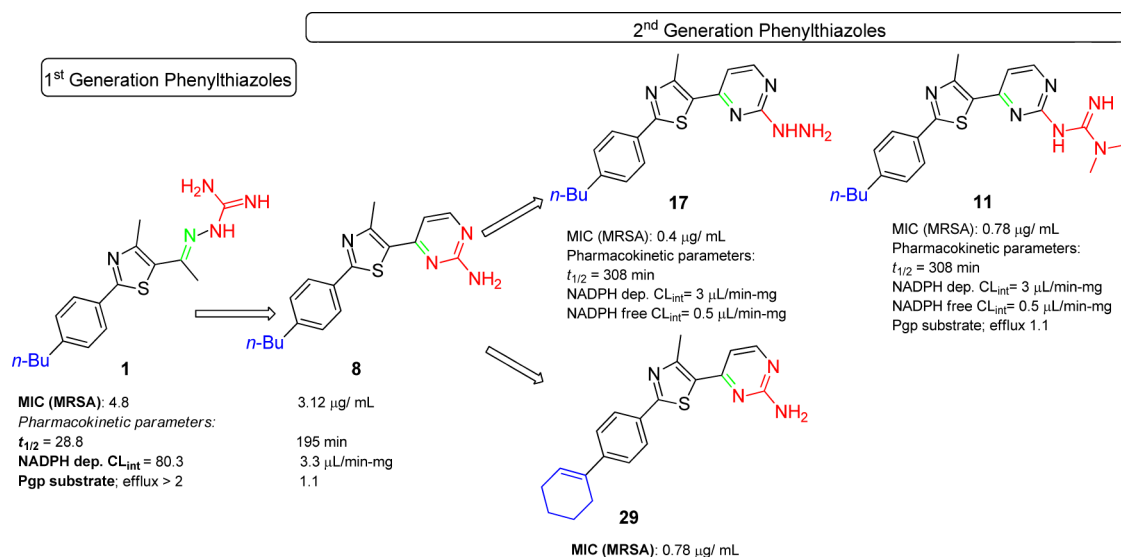


Figure 6. Summary of conclusions.

reported derivatives, is no longer P-glycoprotein substrates and is metabolically stable.

CONCLUSION

In spite of the availability of third- and fourth-generation antibiotics on the market, most of them have fallen prey to the challenge of microbial resistance. The growing threat from multidrug-resistant bacterial pathogens highlights a critical need to expand our currently available arsenal of antibiotics. The recently discovered phenylthiazoles class of antibacterial agents exhibited promising antibacterial effect against several highly resistant strains of *S. aureus*, including MRSA.

Although the first developed phenylthiazoles had a high potency, they were plagued by a short half-life that did not exceed 30 min (due to rapid elimination in human liver microsomes). The main aim of the work described in this article was to develop second-generation analogues with enhanced pharmacokinetic profiles. Thus, the hydrolyzable C=N bond was buried inside a more metabolically stable pyrimidine nucleus. The SAR at the cationic part was then fully examined utilizing various nitrogenous moieties at position-2 of the pyrimidine. Among the tested nitrogenous moieties, hydrazide and *N,N*-dimethylguanidine-containing derivatives **17** and **11** were found to be more potent than vancomycin, the drug of choice for treatment of systemic MRSA infections. By tuning the lipophilic moiety, we found the cyclohexenyl group to be the most active conformationally restricted analogue for the *n*-butyl moiety. Hence, the MIC value of **29** was 1-fold less than that of vancomycin and 4 times better than that of the second-generation lead compound **8** (Figure 6). In addition to the longer $t_{1/2}$ and better expected safety margin, the second-generation phenylthiazoles exhibited a selective advantage over vancomycin in terms of rapid eradication of MRSA cells.

EXPERIMENTAL SECTION

Chemistry. *General.* All biologically tested compounds were of a purity not less than 95%. ^1H NMR spectra were run at 300 MHz, and ^{13}C spectra were determined at 75.46 MHz, in deuterated chloroform (CDCl_3) or dimethyl sulfoxide ($\text{DMSO}-d_6$) on a Varian Mercury VX-300 NMR spectrometer. Chemical shifts are given in parts per million (ppm) on the delta (δ) scale. Chemical shifts were calibrated relative to those of the solvents.³⁵ Flash chromatography was performed on

230–400 mesh silica. The progress of reactions was monitored with Merck silica gel IB2-F plates (0.25 mm thickness). The infrared spectra were recorded in potassium bromide disks on Pye-Unicam SP 3300 and Shimadzu FTIR 8101 PC infrared spectrophotometers. Mass spectra were recorded at 70 eV. High-resolution mass spectra were obtained using a FinniganMAT XL95 instrument. Melting points were determined using capillary tubes with a Stuart SMP30 apparatus and are uncorrected. HPLC analyses were performed on an Agilent binary HPLC system (Model 1260) equipped with a multiple-wavelength UV absorbance detector set for 254 nm, and using a 5 µM C-18 reverse-phase column. All cross-coupling reactions were conducted under nitrogen atmosphere, unless otherwise specified. All yields reported refer to isolated yields. Compounds **3** and **21** were previously reported.²³

(*E*)-1-[2-(4-Butylphenyl)-4-methylthiazol-5-yl]-3-(dimethylamino)prop-2-en-1-one (**4**). To compound **3** (3.1 g, 11.3 mmol) was added DMF-DMA (3 mL), and the reaction mixture was heated at 80 °C for 12 h. After cooling, the formed solid was collected by filtration, washed with petroleum ether and crystallized from ethanol to yield the desired product as an orange solid (3.3 g, 89%), mp = 105.4 °C. ^1H NMR ($\text{DMSO}-d_6$) δ 7.84 (d, J = 8 Hz, 2H), 7.69 (d, J = 12.3 Hz, 1H), 7.31 (d, J = 8.1 Hz, 2H), 5.44 (d, J = 12 Hz, 1H), 3.15 (s, 3H), 2.89 (s, 3H), 2.65 (s, 3H), 2.60 (t, J = 6.8 Hz, 2H), 1.58 (p, J = 4.5 Hz, 2H), 1.32 (m, 2H), 0.88 (t, J = 7.2 Hz, 3H); EIMS m/z 328 (58%).

Potassium Salt of 4-[2-(4-Butylphenyl)-4-methylthiazol-5-yl]-pyrimidine-2-thiolate (**5**). To a solution of potassium hydroxide (200 mg, 3.5 mmol) and thiourea (500 mg, 6.5 mmol) in ethanol (15 mL), enaminone **4** (1 g, 3 mmol) was added. The reaction mixture was heated to reflux for 8 h, and then cooled down in a refrigerator at 8 °C. The formed crystals were filtered and washed with diethyl ether to yield the final product as yellow crystals (1.1 g, 96%), mp > 300 °C. ^1H NMR ($\text{DMSO}-d_6$) δ 8.02 (d, J = 5.1 Hz, 1H), 7.86 (d, J = 7.8 Hz, 2H), 7.32 (d, J = 8.1 Hz, 2H), 6.75 (d, J = 5.4 Hz, 1H), 2.60 (s, 3H), 2.49 (t, J = 5.1 Hz, 2H), 1.55 (m, 2H), 1.32 (m, 2H), 0.91 (t, J = 7.2 Hz, 3H).

2-(4-Butylphenyl)-4-methyl-5-(2-(methylthio)pyrimidin-4-yl)-thiazole (**6**). Method A: To a solution of enaminone **4** (100 mg, 0.3 mmol) in ethanol (10 mL) were added *S*-methylisothiurea hemisulfate salt (160 mg, 0.6 mmol) and anhydrous potassium carbonate (200 mg, 1.4 mmol). The reaction mixture was heated at reflux for 6 h. After completion of reaction, as monitored by TLC, ethanol was evaporated under reduced pressure, and the crude product was purified by flash silica column chromatography using EtOAc–petroleum ether (1:1) to afford white solid (70 mg, 64%), mp = 112.7 °C. EIMS m/z 355 (31), 308 (100).

Method B: To a solution of compound **5** (750 mg, 2.1 mmol) and potassium hydroxide (250 mg, 4.2 mmol) in water (15 mL) was added dimethyl sulfate (0.5 mL, 4 mmol) dropwise with vigorous stirring. After 2 h, the formed solid was filtered and washed with water to yield a yellowish white powder (63 mg, 89%), mp = 112.7 °C. ¹H NMR (DMSO-*d*₆) δ 8.63 (d, *J* = 5.1 Hz, 1H), 7.75 (d, *J* = 7.8 Hz, 2H), 7.44 (d, *J* = 5.1 Hz, 1H), 7.31 (d, *J* = 7.8 Hz, 2H), 2.75 (s, 3H), 2.64 (t, *J* = 7.2 Hz, 2H), 2.55 (s, 3H), 1.58 (p, *J* = 7.2 Hz, 2H), 1.32 (m, 2H), 0.90 (t, *J* = 7.2 Hz, 3H); EIMS *m/z* 355 (31), 308 (100).

2-(4-Butylphenyl)-4-methyl-5-(2-(methylsulfonyl)pyrimidin-4-yl)-thiazole (7). To a solution of compound **6** (500 mg, 1.4 mmol) in dry DCM (5 mL) was added *m*-CPBA (514 mg, 1.7 mmol) in DCM (5 mL) portion-wise with continuous stirring. After the reaction mixture was kept at 23 °C for 16 h, additional DCM (10 mL) was added, and the reaction mixture was washed with 25 mL of a 5% aqueous solution of sodium metabisulfite and 25 mL of 5% aqueous sodium carbonate. The organic layer was separated, dried, and concentrated under reduced pressure to give the desired product as yellow crystals (520 mg, 95%), mp = 100.5 °C. ¹H NMR (DMSO-*d*₆) δ 8.99 (d, *J* = 5.4 Hz, 1H), 8.66 (d, *J* = 5.4 Hz, 1H), 7.89 (d, *J* = 7.8 Hz, 2H), 7.34 (d, *J* = 7.8 Hz, 2H), 2.93 (s, 3H), 2.63 (t, *J* = 7.6 Hz, 2H), 2.61 (s, 3H), 1.57 (p, *J* = 7.6 Hz, 2H), 1.33 (m, 2H), 0.90 (t, *J* = 7.6 Hz, 3H); EIMS *m/z* 387 (12), 308 (100).

Compounds 8–15. To a solution of enaminone **4** (100 mg, 0.3 mmol) in absolute ethanol (5 mL) was added a suitable guanidine or carbimidine (1.2 mmol) and anhydrous potassium carbonate (200 mg, 1.4 mmol). The reaction mixture was heated at reflux for 8 h, ethanol was evaporated under reduced pressure, and the reaction was quenched with cold water (50 mL). The formed flocculated solid was filtered, washed with water, and purified with either acid–base extraction using HCl (1 M, 50 mL) or flash silica column chromatography using EtOAc–petroleum ether–methanol (4.5:4.5:1) to yield the desired products. Physical properties and spectral analysis of isolated products are listed below.

4-[2-(4-Butylphenyl)-4-methylthiazol-5-yl]pyrimidin-2-amine (8). Yellowish-white solid (70 mg, 71%), mp = 159 °C. ¹H NMR (DMSO-*d*₆) δ 8.32 (d, *J* = 5.1 Hz, 1H), 7.86 (d, *J* = 8.1 Hz, 2H), 7.33 (d, *J* = 8.1 Hz, 2H), 6.91 (d, *J* = 5.1 Hz, 1H), 6.74 (brs, 2H), 2.69 (s, 3H), 2.61 (t, *J* = 7.2 Hz, 2H), 1.57 (q, *J* = 7.2 Hz, 2H), 1.32 (q, *J* = 7.2 Hz, 2H), 0.9 (t, *J* = 9.6 Hz, 3H); CIMS *m/z* (rel intensity) 325 (MH⁺, 100); HRMS (EI) *m/z* 324.1421 M⁺, calcd for C₁₈H₂₀N₄S 324.1409; HPLC purity 95.69% (methanol–H₂O, 4:1).

4-[2-(4-Butylphenyl)-4-methylthiazol-5-yl]-N-methylpyrimidin-2-amine (9). White solid (60 mg, 56%), mp = 227 °C (charring). ¹H NMR (DMSO-*d*₆) δ 8.35 (d, *J* = 5.4 Hz, 1H), 7.86 (d, *J* = 7.8 Hz, 2H), 7.50 (brs, 1H), 7.31 (d, *J* = 8.1 Hz, 2H), 6.93 (d, *J* = 5.4 Hz, 1H), 2.72 (s, 3H), 2.64 (t, *J* = 7.5 Hz, 2H), 2.50 (s, 3H), 1.58 (p, *J* = 7.2 Hz, 2H), 1.3 (m, 2H), 0.89 (t, *J* = 7.2 Hz, 3H); CIMS *m/z* (rel intensity) 339 (MH⁺, 100); HRMS (EI) *m/z* 338.1569 M⁺, calcd for C₁₉H₂₂N₄S 338.1565; HPLC purity 97.08% (methanol–H₂O, 4:1).

N-[4-[2-(4-Butylphenyl)-4-methylthiazol-5-yl]pyrimidin-2-yl]-cyanamide (10). White solid (60 g, 28%), mp = 118 °C. IR (KBr) 3383 (NH), 3184, 2935, 2160 cm^{−1}; ¹H NMR (DMSO-*d*₆) δ 8.17 (d, *J* = 5.4 Hz, 1H), 7.91 (d, *J* = 7.8 Hz, 2H), 7.36 (d, *J* = 5.4 Hz, 2H), 6.66 (d, *J* = 4.8 Hz, 1H), 6.55 (brs, 1H), 2.70 (s, 3H), 2.57 (t, *J* = 7.4 Hz, 2H), 1.57 (p, *J* = 7.5 Hz, 2H), 1.31 (six, *J* = 7.5 Hz, 2H), 0.90 (t, *J* = 7.2 Hz, 3H); CIMS *m/z* (rel intensity) 350 (MH⁺, 100); HRMS (EI) *m/z* 349.1375 M⁺, calcd for C₁₉H₁₉N₅S 349.1361; HPLC purity 96.1% (methanol–H₂O, 4:1).

3-[4-[2-(4-Butylphenyl)-4-methylthiazol-5-yl]pyrimidin-2-yl]-1,1-dimethylguanidine (11). Yellowish white solid (55 mg, 46%), mp = 153.7 °C. ¹H NMR (DMSO-*d*₆) δ 8.31 (d, *J* = 7.2 Hz, 1H), 7.85 (d, *J* = 8.4 Hz, 2H), 7.32 (d, *J* = 8.1 Hz, 2H), 7.14 (brs, 1H), 6.84 (d, *J* = 6.4 Hz, 1H), 6.70 (brs, 1H), 3.33 (s, 6H), 2.69 (s, 3H), 2.61 (t, 2H), 1.56 (m, 2H), 1.3 (m, 2H), 0.90 (t, *J* = 7.6 Hz, 3H); CIMS *m/z* (rel intensity) 395 (MH⁺, 100); HRMS (EI) *m/z* 394.1944 M⁺, calcd for C₂₁H₂₆N₆S 394.1940; HPLC purity 95.9% (methanol–H₂O, 4:1).

1-[4-[2-(4-Butylphenyl)-4-methylthiazol-5-yl]pyrimidin-2-yl]-thiourea (12). White solid (78 mg, 33%), mp = 212 °C (charring); ¹H NMR (DMSO-*d*₆) δ 8.33 (d, *J* = 6.8 Hz, 1H), 7.86 (d, *J* = 9.1 Hz, 2H),

7.34 (d, *J* = 9.1 Hz, 2H), 6.91 (d, *J* = 6.8 Hz, 1H), 6.71 (brs, 3H), 2.76 (s, 3H), 2.68 (t, *J* = 7.6 Hz, 2H), 1.55 (m, 2H), 1.32 (m, 2H), 0.90 (t, *J* = 7.2 Hz, 3H); CIMS *m/z* (rel intensity) 384 (MH⁺, 100); HRMS (EI) *m/z* 383.1228 M⁺, calcd for C₁₉H₂₁N₅S₂ 383.1238; HPLC purity 95.01% (methanol–H₂O, 4:1).

2-(4-Butylphenyl)-4-methyl-5-[2-(pyridin-3-yl)pyrimidin-4-yl]-thiazole (13). White solid (50 mg, 23%), mp = 167 °C. ¹H NMR (DMSO-*d*₆) δ 9.68 (s, 1H), 9.37 (d, *J* = 5.1 Hz, 1H), 9.01 (d, *J* = 6.4 Hz, 1H), 7.91 (d, *J* = 6.0 Hz, 1H), 7.89 (d, *J* = 9 Hz, 2H), 7.80 (t, *J* = 6.4 Hz, 1H), 7.31 (d, *J* = 9 Hz, 2H), 7.22 (d, *J* = 5.1 Hz, 1H), 2.83 (s, 3H), 2.60 (t, *J* = 7.2 Hz, 2H), 1.53 (p, *J* = 7.2 Hz, 2H), 1.26 (m, 2H), 0.91 (t, *J* = 7.2 Hz, 3H); EIMS *m/z* (rel intensity) 386 (M⁺, 100); HRMS (EI) *m/z* 386.1560 M⁺, calcd for C₂₃H₂₂N₄S 386.1565; HPLC purity 98.46% (methanol–H₂O, 4:1).

2-(4-Butylphenyl)-5-[2-(1H-pyrazol-1-yl)pyrimidin-4-yl]-4-methylthiazole (14). White solid (55 mg, 46%), mp = 163.7 °C. ¹H NMR (DMSO-*d*₆) δ 8.33 (d, *J* = 5.8 Hz, 1H), 8.03 (d, *J* = 4.8 Hz, 1H), 7.85 (m, 1H), 7.80 (d, *J* = 8.4 Hz, 2H), 7.31 (d, *J* = 8.4 Hz, 2H), 6.87 (d, *J* = 5.1 Hz, 1H), 6.59 (t, *J* = 4.8 Hz, 1H), 2.71 (s, 3H), 2.60 (t, 2H), 1.6 (m, 2H), 1.3 (m, 2H), 0.9 (t, *J* = 6.8 Hz, 3H); EIMS *m/z* (rel intensity) 375 (M⁺, 100), calcd for C₂₁H₂₁N₅S 375; HPLC purity 95.58% (methanol–H₂O, 4:1).

2-(4-Butylphenyl)-4-methyl-5-[2-(pyrrolidin-1-yl)pyrimidin-4-yl]-thiazole (15). Yellowish white solid (0.032 g, 29%), mp = 153.7 °C. ¹H NMR (DMSO-*d*₆) δ 8.40 (d, *J* = 5.4 Hz, 1H), 7.87 (d, *J* = 7.8 Hz, 2H), 7.32 (d, *J* = 7.8 Hz, 2H), 6.88 (d, *J* = 4.8 Hz, 1H), 3.51 (s, 4H), 2.74 (s, 3H), 2.64 (t, *J* = 7.2 Hz, 2H), 1.93 (m, 4H), 1.59 (m, 2H), 1.34 (m, 2H), 0.912 (t, *J* = 7.2 Hz, 3H); CIMS *m/z* (rel intensity) 379 (MH⁺, 100); HRMS (EI) *m/z* 378.1885 M⁺, calcd for C₂₂H₂₆N₄S 378.1878; HPLC purity 97.91% (methanol–H₂O, 4:1).

5-[(1,2,4-Triazolo[1,5-*a*]pyrimidin-5-yl)-2-(4-butylphenyl)-4-methylthiazole (16). To a solution of enaminone **4** (200 mg, 6 mmol) in absolute ethanol (5 mL) were added 4H-1,2,4-triazol-3-amine (100 mg, 0.5 mmol) and anhydrous potassium carbonate (100 mg, 0.7 mmol). The reaction mixture was heated to reflux for 5 h, ethanol was evaporated under reduced pressure, and the reaction was quenched with cold water (50 mL). The formed flocculated solid was filtered, washed with water, and purified with flash silica column chromatography using EtOAc–hexane (1:1) to yield the desired product as a yellowish white solid (55 mg, 52%), mp = 143 °C. ¹H NMR (DMSO-*d*₆) δ 8.95 (d, *J* = 4.8 Hz, 1H), 8.78 (s, 1H), 7.85 (d, *J* = 7.8 Hz, 2H), 7.68 (d, *J* = 4.8 Hz, 1H), 7.24 (d, *J* = 7.8 Hz, 2H), 2.75 (s, 3H), 2.62 (m, 2H), 1.58 (m, 2H), 1.27 (m, 2H), 0.92 (t, *J* = 7.2 Hz, 3H); CIMS *m/z* (rel intensity) 350 (MH⁺, 100); HRMS (EI) *m/z* 349.1375 M⁺, calcd for C₁₉H₁₉N₅S 349.1361; HPLC purity 97.17% (methanol–H₂O, 4:1).

2-(4-Butylphenyl)-5-(2-hydrazinylpyrimidin-4-yl)-4-methylthiazole (17). To a solution of methylsulfonylpyrimidine **7** (100 mg, 0.26 mmol) in DMF (2 mL) was added hydrazine hydrate (5 mL). The reaction mixture was heated at 80 °C for 0.5 h. The formed fluffy solid was filtered and washed with boiled water to remove the residual hydrazine to finally give the title product as a yellowish white fluffy powder (70 mg, 80%), mp = 128 °C. ¹H NMR (DMSO-*d*₆) δ 8.38 (d, *J* = 5.1 Hz, 1H), 8.28 (brs, 1H), 7.87 (d, *J* = 8.1 Hz, 2H), 7.33 (d, *J* = 7.8 Hz, 2H), 6.91 (d, *J* = 6.8 Hz, 1H), 4.22 (brs, 2H), 2.72 (s, 3H), 2.63 (t, *J* = 7.5 Hz, 2H), 1.58 (m, 2H), 1.32 (m, 2H), 0.90 (t, *J* = 7.2 Hz, 3H); CIMS *m/z* (rel intensity) 340 (MH⁺, 100); HRMS (EI) *m/z* 339.1526 M⁺, calcd for C₁₈H₂₁N₅S 339.1518; HPLC purity 97.23% (methanol–H₂O, 4:1).

2-(4-Butylphenyl)-5-(2-guanidinyldiprimidin-4-yl)-4-methylthiazole (18). To a solution of methylsulfonylpyrimidine **7** (100 mg, 0.26 mmol) in dry DMF (5 mL) were added guanidine hydrochloride (50 mg, 0.50 mmol) and potassium carbonate (100 mg, 0.7 mmol). The reaction mixture was heated at 80 °C for 8 h, ethanol was evaporated under reduced pressure, and cold water (10 mL) was added. The formed solid was filtered and crystallized from ethanol (95%) to yield the desired product as a yellowish brown solid (70 mg, 63%), mp = 227.2 °C (charring). ¹H NMR (DMSO-*d*₆) δ 9.98 (brs, 1H), 8.56 (d, *J* = 5.1 Hz, 1H), 8.01 (brs, 2H), 7.65 (d, *J* = 10 Hz, 2H), 7.39 (d, *J* = 8 Hz, 1H), 7.20 (brs, 2H), 7.05 (d, *J* = 7.5 Hz, 2H), 2.50 (s, 3H), 2.43

(m, 2H), 1.42 (m, 2H), 1.19 (m, 2H), 0.77 (t, $J = 7.5$ Hz, 3H); CIMS m/z (rel intensity) 367 (MH^+ , 100); HRMS (EI) m/z 366.1620 M^+ , calcd for $C_{19}H_{22}N_6S$ 366.1627; HPLC purity 99.02% (methanol– H_2O , 4:1).

2-[4-[2-(4-Butylphenyl)-4-methylthiazol-5-yl]pyrimidin-2-yl]-1,1,3,3-tetramethylguanidine (19). To a solution of methylsulfonylpyrimidine 7 (275 mg, 0.7 mmol) in dry DMF (5 mL) were added tetramethylguanidine (0.5 mL) and potassium carbonate (100 mg, 0.7 mmol). The reaction mixture was heated at 80 °C for 8 h and then poured over ice water (50 mL). The formed solid was filtered and purified by flash silica chromatography using EtOAc–hexane (9:1) to yield the desired product as a yellow solid (21 mg, 7%). 1H NMR (DMSO- d_6) δ 8.65 (d, $J = 5.7$ Hz, 1H), 7.90 (d, $J = 8.1$ Hz, 2H), 7.59 (d, $J = 5.1$ Hz, 1H), 7.34 (d, $J = 8.7$ Hz, 2H), 2.70 (s, 12H), 2.63 (m, 2H), 2.57 (s, 3H), 1.57 (p, $J = 6.0$ Hz, 2H), 1.32 (six, $J = 6.0$ Hz, 2H), 0.90 (t, $J = 6.4$ Hz, 3H); EIMS m/z (rel intensity) 422 (M^+ , 31), 407 (100), calcd for $C_{23}H_{30}N_6S$ 422; HPLC purity 95.06% (methanol– H_2O , 4:1).

(E)-3-(Dimethylamino)-1-[2-(4-iodophenyl)-4-methylthiazol-5-yl]prop-2-en-1-one (22). To a solution of compound 21 (1 g, 2.9 mmol) in dry DMF (3 mL) was added DMF–DMA (0.5 mL, 4.5 mmol), and the reaction mixture was heated at 80 °C for 8 h. After cooling down, the reaction mixture was poured over crushed ice with vigorous stirring. The formed orange solid was collected by filtration and washed with water to yield the desired product as an orange solid (1.1 g, 95%), mp = 157 °C. 1H NMR (DMSO- d_6) δ 7.86 (d, $J = 8.1$ Hz, 2H), 7.72 (d, $J = 9.8$ Hz, 2H), 7.71 (d, $J = 12.4$ Hz, 1H), 5.42 (d, $J = 12.8$ Hz, 1H), 3.10 (s, 3H), 2.89 (s, 3H), 2.66 (s, 3H); EIMS m/z (rel intensity) 398 (M^+ , 60), calcd for $C_{15}H_{15}IN_2OS$ 398.

4-[2-(4-Iodophenyl)-4-methylthiazol-5-yl]pyrimidin-2-amine (23). To a solution of enaminone 22 (1.1 g, 2.7 mmol) in absolute ethanol (5 mL) were added guanidine hydrochloride (1 g, 10.5 mmol) and anhydrous potassium carbonate (1.5 g, 10.8 mmol). The reaction mixture was heated at reflux for 12 h. After cooling, the white crystals that formed were filtered and washed with water to yield the desired product as a white solid (0.6 g, 66%), mp = 114.3 °C. 1H NMR (DMSO- d_6) δ 8.33 (d, $J = 5.1$ Hz, 1H), 7.88 (d, $J = 8.8$ Hz, 2H), 7.73 (d, $J = 8.4$ Hz, 2H), 6.91 (d, $J = 5.4$ Hz, 1H), 6.91 (brs, 2H), 2.7 (s, 3H); CIMS m/z (rel intensity) 395 (MH^+ , 100); HRMS (EI) m/z 393.9756 M^+ , calcd for $C_{14}H_{11}IN_4S$ 393.9749; HPLC purity 99.87% (methanol– H_2O , 4:1).

4-[2-(4-Substituted)phenyl]-4-methylthiazol-5-yl]pyrimidin-2-amines (24–26). To a solution of compound 23 (150 mg, 0.43 mmol) in dry DMF (5 mL) were added anhydrous potassium carbonate (250 mg, 1.7 mmol) and a catalytic amount of palladium X-Phos (Xphos Pd G2) (10 mg). The reaction mixture was then charged with the appropriate boronic acid derivative (1.2 equiv). The mixture was irradiated in a SINEO microwave (Uwave-1000) for 1 h at 80 °C, and then the reaction mixture was poured over crushed ice, filtered, and washed with methanol to yield the desired product. The physical characteristics and spectral data of separated products are listed below.

4-[2-[4-(Furan-3-yl)phenyl]-4-methylthiazol-5-yl]pyrimidin-2-amine (24). Yellow solid (100 mg, 78%), mp = 161.2 °C. 1H NMR (DMSO- d_6) δ 8.33 (m, 1H), 8.31 (s, 1H), 7.97 (d, $J = 8.1$ Hz, 2H), 7.75 (d, $J = 8.4$ Hz, 2H), 7.04 (m, 1H), 6.92 (m, 2H), 6.73 (brs, 2H), 2.71 (s, 3H); CIMS m/z (rel intensity) 335 (MH^+ , 100); HRMS (EI) m/z 334.0892 M^+ , calcd for $C_{18}H_{14}N_4OS$ 334.0888; HPLC purity 99.1% (methanol– H_2O , 4:1).

4-[2-[4-(Furan-2-yl)phenyl]-4-methylthiazol-5-yl]pyrimidin-2-amine (25). Brown solid (105 mg, 82%), mp = 209.3 °C. 1H NMR (DMSO- d_6) δ 8.33 (d, $J = 6.1$ Hz, 1H), 8.01 (d, $J = 8.6$ Hz, 2H), 7.83 (m, 3H), 7.10 (d, $J = 3$ Hz, 1H), 6.92 (d, $J = 4.8$ Hz, 1H), 6.73 (brs, 2H), 6.65 (dd, $J = 4.5, 4.8$ Hz, 1H), 2.70 (s, 3H); CIMS m/z (rel intensity) 335 (MH^+ , 100); HRMS (EI) m/z 334.0898 M^+ , calcd for $C_{18}H_{14}N_4OS$ 334.0888; HPLC purity 98.75% (methanol– H_2O , 4:1).

4-[4-Methyl-2-[4-(thiophen-3-yl)phenyl]thiazol-5-yl]pyrimidin-2-amine (26). Brown solid (120 mg, 90%), mp = 225 °C (charring). 1H NMR (DMSO- d_6) δ 8.33 (d, $J = 5.1$ Hz, 1H), 7.99 (m, 3H), 7.86 (d, $J = 8.4$ Hz, 2H), 7.67 (d, $J = 2.7$ Hz, 1H), 7.63 (d, $J = 3.9$ Hz, 1H), 6.91 (d, $J = 5.1$ Hz, 1H), 6.73 (brs, 2H), 2.71 (s, 3H); CIMS m/z (rel

intensity) 351 (MH^+ , 100); HRMS (EI) m/z 350.0670 M^+ , calcd for $C_{18}H_{14}N_4S_2$ 350.0660; HPLC purity 98.97% (methanol– H_2O , 4:1).

4-[2-[4-(Cycloalkenyl)phenyl]-4-methylthiazol-5-yl]pyrimidin-2-amines (27–35). To a solution of compound 23 (150 mg, 0.43 mmol) in dry DMF (5 mL) were added triethylamine (0.2 mL, 1.9 mmol) and a catalytic amount of palladium acetate (20 mg). The flask was then charged with an appropriate cycloalkene (2.4 mmol). The mixture was heated at 80 °C for 1 h, and then was filtered through Celite 545, extracted with ethyl acetate, and purified with flash silica column chromatography using eluent EtOAc–hexane (1:9) to yield the desired product as presented below.

4-[2-[4-(Cyclopent-1-en-1-yl)phenyl]-4-methylthiazol-5-yl]pyrimidin-2-amine (27). Off-white solid (50 mg, 39%), mp = 160.6 °C. 1H NMR (DMSO- d_6) δ 8.33 (d, $J = 5.4$ Hz, 1H), 7.89 (d, $J = 7.8$ Hz, 2H), 7.31 (d, $J = 7.8$ Hz, 2H), 6.91 (d, $J = 5.4$ Hz, 1H), 6.71 (brs, 2H), 5.81 (d, $J = 1.5$ Hz, 1H), 2.70 (s, 3H), 1.69–1.48 (m, 2H), 1.23–1.54 (m, 2H), 0.85–0.78 (m, 2H); CIMS m/z (rel intensity) 335 (MH^+ , 100); HRMS (EI) m/z 334.1250 M^+ , calcd for $C_{19}H_{18}N_4S$ 334.1252; HPLC purity 97.51% (methanol– H_2O , 4:1).

4-[4-Methyl-2-[4-(4-methylcyclopent-1-en-1-yl)phenyl]thiazol-5-yl]pyrimidin-2-amine (28). Off-white solid (60 mg, 45%), mp = 141 °C. 1H NMR (DMSO- d_6) δ 8.32 (d, $J = 5.1$ Hz, 1H), 7.89 (d, $J = 7.8$ Hz, 2H), 7.52 (d, $J = 7.8$ Hz, 2H), 6.90 (d, $J = 5.1$ Hz, 1H), 6.72 (brs, 2H), 5.84 (m, 1H), 2.70 (s, 3H), 1.28–1.69 (m, 4H), 0.92 (d, $J = 6.3$ Hz, 3H), 0.85 (m, 1H); CIMS m/z (rel intensity) 349 (MH^+ , 100); HRMS (EI) m/z 348.1401 M^+ , calcd for $C_{20}H_{20}N_4S$ 348.1409; HPLC purity 97.29% (methanol– H_2O , 4:1).

4-[2-[4-(Cyclohex-1-en-1-yl)phenyl]-4-methylthiazol-5-yl]pyrimidin-2-amine (29). Off-white solid (65 mg, 49%), mp = 140.4 °C. 1H NMR (DMSO- d_6) δ 8.32 (d, $J = 4.8$ Hz, 1H), 7.89 (d, $J = 7.8$ Hz, 2H), 7.39 (d, $J = 7.8$ Hz, 2H), 6.91 (d, $J = 4.8$ Hz, 1H), 6.80 (brs, 2H), 5.76 (d, $J = 1.5$ Hz, 1H), 2.69 (s, 3H), 2.77–1.84 (m, 4H), 1.23–1.17 (m, 4H); CIMS m/z (rel intensity) 349 (MH^+ , 100); HRMS (EI) m/z 348.1414 M^+ , calcd for $C_{20}H_{20}N_4S$ 348.1409; HPLC purity 96.64% (methanol– H_2O , 4:1).

4-[2-[4-(Cyclohept-1-en-1-yl)phenyl]-4-methylthiazol-5-yl]pyrimidin-2-amine (30). Off-white solid (100 mg, 73%), mp = 164 °C. 1H NMR (DMSO- d_6) δ 8.32 (d, $J = 4.8$ Hz, 1H), 7.89 (d, $J = 7.8$ Hz, 2H), 7.36 (d, $J = 7.8$ Hz, 2H), 6.90 (d, $J = 4.8$ Hz, 1H), 6.71 (brs, 2H), 5.86 (m, 1H), 2.69 (s, 3H), 2.69 (m, 2H), 2.263–2.15 (m, 2H), 1.85–1.71 (m, 2H), 1.49–1.38 (m, 2H), 1.22 (m, 2H); CIMS m/z (rel intensity) 363 (MH^+ , 100); HRMS (EI) m/z 362.1579 M^+ , calcd for $C_{21}H_{22}N_4S$ 362.1565; HPLC purity 98.09% (methanol– H_2O , 4:1).

4-[2-[4-(Cyclooct-1-en-1-yl)phenyl]-4-methylthiazol-5-yl]pyrimidin-2-amine (31). Off-white solid (120 mg, 84%), mp = 188 °C. 1H NMR (DMSO- d_6) δ 8.32 (d, $J = 5.1$ Hz, 1H), 7.89 (d, $J = 7.8$ Hz, 2H), 7.37 (d, $J = 7.8$ Hz, 2H), 6.90 (d, $J = 5.1$ Hz, 1H), 6.72 (brs, 2H), 5.71 (m, 1H), 2.69 (s, 3H), 2.28 (m, 2H), 1.75–1.48 (m, 10H); CIMS m/z (rel intensity) 377 (MH^+ , 100); HRMS (EI) m/z 376.1719 M^+ , calcd for $C_{22}H_{24}N_4S$ 376.1722; HPLC purity 95.98% (methanol– H_2O , 4:1).

4-[2-[4-(Cyclopentylidenemethyl)phenyl]-4-methylthiazol-5-yl]pyrimidin-2-amine (32). Yellowish white solid (55 mg, 41%), mp = 143 °C. 1H NMR (DMSO- d_6) δ 8.33 (d, $J = 5.4$ Hz, 1H), 7.88 (d, $J = 8.4$ Hz, 2H), 7.30 (d, $J = 8.4$ Hz, 2H), 6.90 (d, $J = 5.4$ Hz, 1H), 6.71 (brs, 2H), 5.38 (s, 1H), 2.70 (s, 3H), 2.27 (m, 1H), 2.16 (m, 1H), 1.82 (m, 2H), 1.22 (m, 4H); CIMS m/z (rel intensity) 349 (MH^+ , 100); HRMS (EI) m/z 348.1420 M^+ , calcd for $C_{20}H_{20}N_4S$ 348.1409; HPLC purity 96.18% (methanol– H_2O , 4:1).

4-[2-[4-(Cyclohexylidenemethyl)phenyl]-4-methylthiazol-5-yl]pyrimidin-2-amine (33). Brown solid (60 mg, 44%), mp = 165 °C. 1H NMR (DMSO- d_6) δ 8.33 (d, $J = 5.4$ Hz, 1H), 7.91 (d, $J = 8.4$ Hz, 2H), 7.33 (d, $J = 8.4$ Hz, 2H), 6.91 (d, $J = 5.4$ Hz, 1H), 6.72 (brs, 2H), 6.27 (s, 1H), 2.71 (s, 3H), 2.48 (m, 1H), 2.40 (m, 1H), 1.98–1.23 (m, 6H), 1.05 (m, 2H); CIMS m/z (rel intensity) 363 (MH^+ , 100); HRMS (EI) m/z 362.1570 M^+ , calcd for $C_{21}H_{22}N_4S$ 362.1565; HPLC purity 99.72% (methanol– H_2O , 4:1).

(E)-4-[2-[4-(2-Cyclopentylvinyl)phenyl]-4-methylthiazol-5-yl]pyrimidin-2-amine (34). Brown solid (40 mg, 29%), mp = 180.7 °C. 1H NMR (DMSO- d_6) δ 8.32 (d, $J = 5.4$ Hz, 1H), 7.88 (d, $J = 8.1$ Hz, 2H), 7.51 (d, $J = 8.1$ Hz, 2H), 7.31 (dd, $J = 12, 6.8$ Hz, 1H), 6.90 (d, J

= 5.4 Hz, 1H), 6.71 (brs, 2H), 6.44 (d, J = 12.0 Hz, 1H), 2.69 (s, 3H), 2.21 (t, J = 6 Hz, 1H), 1.95 (sep, J = 7.5 Hz, 1H), 1.79–1.71 (m, 1H), 1.62–1.45 (m, 4H), 1.22–1.15 (m, 2H); CIMS m/z (rel intensity) 363 (MH⁺, 100); HRMS (EI) m/z 362.1559 M⁺, calcd for C₂₁H₂₂N₄S 362.1565; HPLC purity 95.33% (methanol–H₂O, 4:1).

(E)-4-{2-[4-(2-Cyclohexylvinyl)phenyl]-4-methylthiazol-5-yl}pyrimidin-2-amine (**35**). Brown solid (65 mg, 45%), mp = 189 °C. ¹H NMR (DMSO-*d*₆) δ 8.32 (d, J = 5.0 Hz, 1H), 7.95 (m, 1H), 7.88 (d, J = 7.8 Hz, 2H), 7.51 (d, J = 7.8 Hz, 2H), 6.90 (d, J = 4.8 Hz, 1H), 6.80 (brs, 2H), 6.41 (m, 1H), 2.69 (s, 3H), 2.17 (m, 1H), 1.74 (m, 2H), 1.54–1.49 (m, 4H), 1.22–1.14 (m, 4H); CIMS m/z (rel intensity) 377 (MH⁺, 100); HRMS (EI) m/z 376.1731 M⁺, calcd for C₂₂H₂₄N₄S 376.1722; HPLC purity 95.03% (methanol–H₂O, 4:1).

Antimicrobial Testing. Determination of Minimum Inhibitory Concentration (MIC). MRSA clinical isolates and vancomycin-resistant *Staphylococcus aureus* (VRSA) strain were obtained through the Network of Antimicrobial Resistance in *Staphylococcus aureus* (NARSA) program. In addition, vancomycin-resistant *Enterococcus faecium* (VRE) strain was obtained from the ATCC.

The MICs of the newly synthesized compounds, tested against isolates of *S. aureus* and VRE, were determined using the broth microdilution method in accordance with the recommendations contained in the Clinical and Laboratory Standards Institute guidelines.³⁴ Bacteria were cultured in cation-adjusted Mueller Hinton broth in a 96-well plate. Compounds, using triplicate samples, were added to the plate and serially diluted. Plates were incubated at 37 °C for 20 h prior to determining the MIC. Plates were visually inspected, and the MIC was categorized as the concentration at which no visible growth of bacteria was observed. The average of triplicate MIC determinations is reported.

Time–Kill Assay. MRSA (USA300) cells, in the logarithmic growth phase, were diluted to 1.0×10^6 CFU/mL and exposed to concentrations equivalent to $3.0 \times \text{MIC}$ (in triplicate) of tested compounds, and vancomycin in tryptic soy broth (Becton, Dickinson and Company, Sparks, MD, USA). Aliquots (100 μ L) were taken from each sample after 2, 4, 6, 8, 10, 12, and 24 h, serially diluted in PBS, and transferred to trypticase soy agar (Becton, Dickinson and Company) plates. Plates were incubated at 37 °C for at least 16 h before counting viable CFU/mL to determine the time required to reduce the bacterial cell count by 3 log₁₀.

In Vitro Cytotoxicity Analysis. Compound 17 was assayed at concentrations of 8, 16, 32, 64, 128, and 256 μ g/mL against an immortal keratinocyte cell line (HaCaT) in order to determine the potential toxic effect against mammalian cells *in vitro*. Cells were cultured in Dulbecco's modified Eagle's medium (Sigma-Aldrich, St. Louis, MO, USA) with 10% fetal bovine serum (USA Scientific, Inc.) at 37 °C with 5% CO₂. Controls received DMSO alone at a concentration equal to that in drug-treated cell samples. The cells were incubated with the compounds in a 96-well plate at 37 °C and 5.0% CO₂ for 2 h prior to addition of the assay reagent MTS (Promega, Madison, WI, USA). Corrected absorbance readings (actual absorbance readings for each treatment subtracted from background absorbance) were taken using a kinetic ELISA microplate reader (Molecular Devices, Sunnyvale, CA, USA). The quantity of viable cells after treatment with each compound is expressed as a percentage of the control, DMSO.

Pharmacokinetic Assays. Caco-2 Permeability Assay. Caco-2 cells grown in tissue culture flasks were trypsinized and suspended in medium, and the suspensions were applied to wells of a Millipore 96-well Caco-2 plate. The cells were allowed to grow and differentiate for 3 weeks, feeding at 2-day intervals. For apical-to-basolateral (A→B) permeability, the tested compound was added to the apical (A) side, and the amount of permeation was determined on the basolateral (B) side; for basolateral-to-apical (B→A) permeability, the tested compound was added to the B side, and the amount of permeation was determined on the A side. The A-side buffer contained 100 μ M Lucifer yellow dye, in transport buffer (1.98 g/L glucose in 10 mM HEPES, 1.0 \times Hank's Balanced Salt Solution), pH 6.5, and the B-side buffer contained transport buffer at pH 7.4. Caco-2 cells were incubated with these buffers for 2 h, and the receiver-side buffer was

removed for analysis by LC/MS/MS. To verify that the Caco-2 cell monolayers were properly formed, aliquots of the cell buffers were analyzed by fluorescence to determine the transport of the impermeable Lucifer yellow dye. Any deviations from control values are reported. Data are expressed as permeability $P_{\text{app}} = (dQ/dt)/C_0A$, where dQ/dt is the rate of permeation, C_0 is the initial concentration of test agent, and A is the area of the monolayer. In bidirectional permeability studies, the efflux ratio is also calculated: $R_E = P_{\text{app}}(\text{B} \rightarrow \text{A})/P_{\text{app}}(\text{A} \rightarrow \text{B})$. An $R_E > 2$ indicates a potential substrate for P-glycoprotein or other active efflux transporters.

PBS Solubility Screen. Serial dilutions of the tested compounds, reserpine, tamoxifen, and verapamil were prepared in phosphate-buffered saline (PBS) at 100 \times the final concentration. The solutions were diluted 100-fold into PBS in a 96-well plate and mixed. The absorbance of the PBS-containing plate was measured prior to addition of the test agents to determine the background absorbance. After 2 h, the presence of precipitate was detected by turbidity (absorbance at 540 nm). An absorbance value of greater than (mean + 3 \times standard deviation of the blank), after subtracting the pre-experiment background, is indicative of turbidity. The solubility limit is reported as the highest experimental concentration with no evidence of turbidity.

Human Microsomal Stability Analysis. The tested compounds were incubated in duplicate with human liver microsomes at 37 °C. The reaction contained microsomal protein in 100 mM potassium phosphate, 2 mM NADPH, 3 mM MgCl₂, pH 7.4. A control was run for each test agent omitting NADPH to detect NADPH-free degradation. At 0, 10, 20, 40, and 60 min, an aliquot was removed from each experimental and control reaction and mixed with an equal volume of ice-cold stop solution (methanol containing haloperidol, diclofenac, or other internal standard). Stopped reactions were incubated at least 10 min at –20 °C, and an additional volume of water was added. The samples were centrifuged to remove precipitated protein, and the supernatants were analyzed by LC/MS/MS to quantitate the remaining parent. Data are converted to % remaining by dividing by the time zero concentration value. Data are fit to a first-order decay model to determine half-life. Intrinsic clearance is calculated from the half-life and the protein concentrations: $\text{CL}_{\text{int}} = \ln(2)/T_{1/2}[\text{microsomal protein}]$.

Statistical Analysis. All statistical analysis was conducted using Kaleida Graph, version 4.03 (Synergy Software, Reading, PA). Statistical significance was determined using ANOVA and the Fisher's least significant difference test with $\alpha = 0.05$.

In Vivo Pharmacokinetics. This assay was conducted at an accredited bioequivalence center (http://www.grc-me.com/pk_pd.html). Pharmacokinetic studies were performed in male naïve Sprague–Dawley (SD) rats (three animals) following Institutional Animal Care and Use Committee guidelines. Oral dosing was administered by gavage in a vehicle containing 5% ethanol, 45% PEG 400, and 50% water. Blood samples were collected over a 24 h period post dose into Vacutainer tubes containing EDTA-K2. Plasma was isolated, and the concentration of compound 17 in plasma was determined by LC/MS/MS after protein precipitation with acetonitrile.

Non-compartmental PK analysis was performed on plasma concentration data to calculate PK parameters using Kinetica 2000 (release 4.4.1).

■ ASSOCIATED CONTENT

● Supporting Information

The Supporting Information is available free of charge on the ACS Publications website at DOI: 10.1021/acs.jmedchem.6b00233.

Molecular formulas for 2–35 (CSV)

■ AUTHOR INFORMATION

Corresponding Author

*Phone: 0020-100-771-5002. E-mail: amayhoub@azhar.edu.eg.

Notes

The authors declare no competing financial interest.

ACKNOWLEDGMENTS

This work was supported by the Academy of Scientific Research & Technology, Egypt, JESOUR-D program (Grant ID No. 42). The authors also acknowledge The World Academy of Sciences, COMSTECH-TWAS program (grant no. 14-389 RG/PHA/AF/AC_C) for their generous support.

ABBREVIATIONS USED

Caco-2, heterogeneous human epithelial colorectal adenocarcinoma cells; CA-MRSA, community-acquired MRSA; CFUs, colony-forming units; C_{max} , maximum serum concentration; DMF-DMA, dimethylformamide–dimethylacetal; HaCaT, human keratinocytes; MRSA, methicillin-resistant *Staphylococcus aureus*; MRT, mean residence time; P_{app} , apparent permeability; PK, pharmacokinetic; SSTIs, skin and soft tissue infections; VISA, vancomycin-intermediate *S. aureus*

REFERENCES

- (1) Davies, J.; Davies, D. Origins and evolution of antibiotic resistance. *Microbiol. Mol. Biol. Rev.* **2010**, *74*, 417–433.
- (2) Kirby, W. M. Extraction of a highly potent penicillin inactivator from penicillin resistant staphylococci. *Science* **1944**, *99*, 452–453.
- (3) Barber, M.; Rozwadowska-Dowzenko, M. Infection by penicillin-resistant staphylococci. *Lancet* **1948**, *252*, 641–644.
- (4) Rountree, P. M.; Freeman, B. M. Infections caused by a particular phage type of *Staphylococcus aureus*. *Med. J. Aust.* **1955**, *42*, 157–161.
- (5) Jevons, M. P. Celbenin[®] – resistant *Staphylococci*. *Br. Med. J.* **1961**, *1*, 124–125.
- (6) Peacock, J. E., Jr.; Marsik, F. J.; Wenzel, R. P. Methicillin-resistant *Staphylococcus aureus*: introduction and spread within a hospital. *Ann. Intern. Med.* **1980**, *93*, 526–532.
- (7) Crossley, K.; Landesman, B.; Zaske, D. An outbreak of infections caused by strains of *Staphylococcus aureus* resistant to methicillin and aminoglycosides. II. Epidemiologic studies. *J. Infect. Dis.* **1979**, *139*, 280–287.
- (8) Fischbach, M. A.; Walsh, C. T. Antibiotics for emerging pathogens. *Science* **2009**, *325*, 1089–1093.
- (9) Borg, M. A.; de Kraker, M.; Scicluna, E.; van de Sande-Bruinsma, N.; Tiemersma, E.; Monen, J.; Grundmann, H. Prevalence of methicillin-resistant *Staphylococcus aureus* (MRSA) in invasive isolates from southern and eastern Mediterranean countries. *J. Antimicrob. Chemother.* **2007**, *60*, 1310–1315.
- (10) Ahmad, M. K.; Asrar, A. Prevalence of methicillin resistant *Staphylococcus aureus* in pyogenic community and hospital acquired skin and soft tissues infections. *JPMA J. Pak. Med. Assoc.* **2014**, *64*, 892–895.
- (11) Hiramatsu, K.; Aritaka, N.; Hanaki, H.; Kawasaki, S.; Hosoda, Y.; Hori, S.; Fukuchi, Y.; Kobayashi, I. Dissemination in Japanese hospitals of strains of *Staphylococcus aureus* heterogeneously resistant to vancomycin. *Lancet* **1997**, *350*, 1670–1673.
- (12) Weigel, L. M.; Clewell, D. B.; Gill, S. R.; Clark, N. C.; McDougal, L. K.; Flannagan, S. E.; Kolonay, J. F.; Shetty, J.; Killgore, G. E.; Tenover, F. C. Genetic analysis of a high-level vancomycin-resistant isolate of *Staphylococcus aureus*. *Science* **2003**, *302*, 1569–1571.
- (13) Hawkins, C.; Huang, J.; Jin, N.; Noskin, G. A.; Zembower, T. R.; Bolon, M. Persistent *Staphylococcus aureus* bacteremia: an analysis of risk factors and outcomes. *Arch. Intern. Med.* **2007**, *167*, 1861–1867.
- (14) Khatib, R.; Johnson, L.; Sharma, M.; Fakih, M.; Ganga, R.; Riederer, K. Persistent *Staphylococcus aureus* bacteremia: incidence and outcome trends over time. *Scand. J. Infect. Dis.* **2009**, *41*, 4–9.
- (15) Dombrowski, J. C.; Winston, L. G. Clinical failures of appropriately-treated methicillin-resistant *Staphylococcus aureus* infections. *J. Infect.* **2008**, *57*, 110–115.
- (16) Lodise, T. P.; Lomaestro, B.; Graves, J.; Drusano, G. L. Larger vancomycin doses (at least four grams per day) are associated with an increased incidence of nephrotoxicity. *Antimicrob. Agents Chemother.* **2008**, *52*, 1330–1336.
- (17) Wang, G.; Hindler, J. F.; Ward, K. W.; Bruckner, D. A. Increased vancomycin MICs for *Staphylococcus aureus* clinical isolates from a university hospital during a 5-year period. *J. Clin. Microbiol.* **2006**, *44*, 3883–3886.
- (18) Chambers, H. F. Community-associated MRSA-resistance and virulence converge. *N. Engl. J. Med.* **2005**, *352*, 1485–1487.
- (19) Moran, G. J.; Krishnadasan, A.; Gorwitz, R. J.; Fosheim, G. E.; McDougal, L. K.; Carey, R. B.; Talan, D. A. Methicillin-resistant *S. aureus* infections among patients in the emergency department. *N. Engl. J. Med.* **2006**, *355*, 666–674.
- (20) Frazee, B. W.; Lynn, J.; Charlebois, E. D.; Lambert, L.; Lowery, D.; Perdreau-Remington, F. High prevalence of methicillin-resistant *Staphylococcus aureus* in emergency department skin and soft tissue infections. *Ann. Emerg. Med.* **2005**, *45*, 311–320.
- (21) Fridkin, S. K.; Hageman, J. C.; Morrison, M.; Sanza, L. T.; Como-Sabetti, K.; Jernigan, J. A.; Harriman, K.; Harrison, L. H.; Lynfield, R.; Farley, M. M. Methicillin-resistant *Staphylococcus aureus* disease in three communities. *N. Engl. J. Med.* **2005**, *352*, 1436–1444.
- (22) Moran, G. J.; Amii, R. N.; Abrahamian, F. M.; Talan, D. A. Methicillin-resistant *Staphylococcus aureus* in community-acquired skin infections. *Emerging Infect. Dis.* **2005**, *11*, 928–930.
- (23) Mohammad, H.; Mayhoub, A. S.; Ghafoor, A.; Soofi, M.; Alajlouni, R. A.; Cushman, M.; Seleem, M. N. Discovery and characterization of potent thiazoles versus methicillin- and vancomycin-resistant *Staphylococcus aureus*. *J. Med. Chem.* **2014**, *57*, 1609–1615.
- (24) French, G. L. Bactericidal agents in the treatment of MRSA infections-the potential role of daptomycin. *J. Antimicrob. Chemother.* **2006**, *58*, 1107–1117.
- (25) Pankey, G. A.; Sabath, L. D. Clinical relevance of bacteriostatic versus bactericidal mechanisms of action in the treatment of Gram-positive bacterial infections. *Clin. Infect. Dis.* **2004**, *38*, 864–870.
- (26) Mohammad, H.; Cushman, M.; Seleem, M. N. Antibacterial evaluation of synthetic thiazole compounds in vitro and in vivo in a methicillin-resistant *Staphylococcus aureus* (MRSA) skin infection mouse model. *PLoS One* **2015**, *10*, e0142321.
- (27) Mohammad, H.; Mayhoub, A. S.; Cushman, M.; Seleem, M. N. Anti-biofilm activity and synergism of novel thiazole compounds with glycopeptide antibiotics against multidrug-resistant *Staphylococci*. *J. Antibiot.* **2015**, *68*, 259–266.
- (28) Mohammad, H.; Reddy, P. V.; Monteleone, D.; Mayhoub, A. S.; Cushman, M.; Seleem, M. N. Synthesis and antibacterial evaluation of a novel series of synthetic phenylthiazole compounds against methicillin-resistant *Staphylococcus aureus* (MRSA). *Eur. J. Med. Chem.* **2015**, *94*, 306–316.
- (29) Singh, S. R.; Bacon, A. E., 3rd; Young, D. C.; Couch, K. A. In vitro 24-h time-kill studies of vancomycin and linezolid in combination versus methicillin-resistant *Staphylococcus aureus*. *Antimicrob. Agents Chemother.* **2009**, *53*, 4495–4497.
- (30) Vergidis, P.; Rouse, M. S.; Euba, G.; Karau, M. J.; Schmidt, S. M.; Mandrekar, J. N.; Steckelberg, J. M.; Patel, R. Treatment with linezolid or vancomycin in combination with rifampin is effective in an animal model of methicillin-resistant *Staphylococcus aureus* foreign body osteomyelitis. *Antimicrob. Agents Chemother.* **2011**, *55*, 1182–1186.
- (31) King, M. D.; Humphrey, B. J.; Wang, Y. F.; Kourbatova, E. V.; Ray, S. M.; Blumberg, H. M. Emergence of community-acquired methicillin-resistant *Staphylococcus aureus* USA 300 clone as the predominant cause of skin and soft-tissue infections. *Ann. Intern. Med.* **2006**, *144*, 309–317.
- (32) Ghasemzadeh-Moghaddam, H.; Neela, V.; Goering, R.; Mariana, N. S. Methicillin sensitive *Staphylococcus aureus* (MSSA) isolates as a potential source for the emergence of USA 300 methicillin resistant *Staphylococcus aureus* (MRSA) in Malaysia. *Asian Pac. J. Trop. Biomed.* **2012**, *29*, 429–433.

(33) Crooks, N.; Ross, T.; Grant, S.; Anmolsingh, R.; Gabriel, A.; Foggo-Osseyran, A.; Carroll, K.; Wilson, C. A severe pneumonia due to methicillin resistant *Staphylococcus aureus* clone USA 300: implications of vertical transmission. *West Indian Med. J.* **2012**, *61*, 145–147.

(34) *Methods for Dilution Antimicrobial Susceptibility Tests for Bacteria That Grow Aerobically*, 7th ed.; Approved Standard M7-A7; Clinical and Laboratory Standards Institute: Wayne, PA, 2006.

(35) Gottlieb, H. E.; Kotlyar, V.; Nudelman, A. NMR chemical shifts of common laboratory solvents as trace impurities. *J. Org. Chem.* **1997**, *62*, 7512–7515.